Simulation of the Asian Monsoon by IAP AGCM Coupled with an Advanced Land Surface Model (IAP94)

Zeng Qingcun (曾庆存), *Dai Yongjiu* (戴永久)
and *Xue Feng* (薛 峰)
Institute of Atmospheric Physics, Chinese Academy of Sciences, Beijing 100080
Received May 23, 1997; revised August 25, 1997

ABSTRACT

In this paper, the global and regional features of the seasonal variation of general circulation, and especially the Asian monsoon simulated by the Institute of Atmospheric Physics Two-level AGCM coupled with a sophisticated land-surface model (IAP94-GCM) are presented and compared with the observation. The comparison is made by using the equilibrium multiyear seasonal cycle climate from a 100-year integration. In the integration sea surface temperature (SST) and sea ice are taken from the observed climatological data (with seasonal variation) because our purpose is to see the improvement of simulation due to the coupling with an advanced land surface model.

Overall, the IAP94-GCM provides a reasonably realistic simulation of the interseasonal and intraseasonal climatology of the Asian monsoon and yields an important information that sheds light on the thermal underpinning and the thermodynamics of the seasonal and even multiscale variabilities associated with the Asian summer monsoon.

Key words: Advanced Land Surface Model, Coupled Model, Simulation, Asian Monsoon

1. INTRODUCTION

It is well recognized that the correct representation of the land surface characteristics and their temporal variations is important to improve the simulation of climate, especially the surface and low-level atmospheric variables (see, for example, Dai and Zeng, 1997; Dai, Xue and Zeng, 1997). In recent years a sophisticated land-surface scheme, the Institute of Atmospheric Physics land surface model (IAP94), has been developed and coupled with the IAP two-level AGCM. This coupled model has been integrated up to 100 years. So that the mean fields of the last 25 years integrations can be well considered as an equilibrium climate of the model. The analyses of the global and some characteristic regional features of this model climate have been described in our previous paper (Dai, Xue and Zeng, 1997). In this paper, we will focus our attention on the analyses of the features of the simulated Asian summer monsoon circulation and its temporal evolution. Our main effort will be devoted to evaluating the ability of this coupled model to simulate the most important but difficult to be well simulated elements such as the monsoon rain belt pattern, the surface temperature, hydrology and heat fluxes in the Asian summer monsoon regions and exploring and understanding the importance of land surface processes.

A slightly earlier, Meehl (1994) studied the influence of land surface on the Asian summer monsoon by GCMs' sensitivity experiments and identified the importance of land surface processes, the results were further confirmed by observational study (Li and Yanai, 1996). In particular, the linkage between Eurasian winter snow cover and Asian summer monsoon has

been widely investigated by GCMs sensitivity experiments (Barnett et al., 1989; Yasunari et al., 1991; Vernekar et al., 1995; Douville and Royer, 1996). Lin, Zeng and Ouyang (1996) have also carried out sensitivity studies on the important role of the surface characteristics in the simulation of Asian monsoon by replacing the old formulation of surface albedo in IAP AGCM by the observed one, and the results have shown an impressive improvement of the simulation. In summary, all these studies expressed an expectation of the improved simulation of land surface hydrological and thermal processes by the more or less improved model.

Table 1. The IAP94 AGCM

Forecast variables	Horizontal velocity, temperature, water vapor mixing ratio, surface pressure, surface temperature, ground wetness, and snow amount
Vertical representation	*Normalized pressure coordinate, two* interior tropospheric levels
Horizontal representation	C-grid system, available energy conservation finite-difference scheme (Zeng and Zhang, 1987)
Time integration	*Semi-implicit, Matsuno time integrator with* Shuman and Mesinger averaging technique
Orography and surface type	Orography based on the data of Gates and Nelson (1975); the SiB global archive of land cover (Dorman and Sellers, 1989); the archive of soil color, texture, and drainage established by Wilson (1985), (but the land cover in China is replaced by Chinese results)
Radiation	Solar radiation based on the delta-Eddington model (Cess, 1985; Cess and Potter, 1987); longwave radiation based on Katayama scheme (1972)
Surface albedo	Aggregated parameterization scheme (Dai and Zeng, 1997)
Horizontal diffusion	Two-dimensional non-linear diffusion (Smagorinsky, 1963)
Cumulus Convection	Scheme of Arakawa et al. (1969)
Precipitation	Precipitation resulted from large-scale condensation and from middle-level and penetrating convection
Land surface processes	Including a detailed description for the processes of vegetation, snow and soil (Dai and Zeng, 1997)
Sea surface temperature	Climatology, averaged 1979-1988, or 1979-1988 AMIP SST

Generally speaking, our land-surface model (IAP94) is a comprehensive one which consists of a detailed soil, snow cover and vegetation canopy. This model has been validated by various off-line experiments participating the active Project for Intercomparison of Land-surface Parameterization Schemes (PILPS). After that the land surface model IAP94 has been coupled to the IAP two-level AGCM (hereafter referred to as IAP94-GCM) and successfully integrated for 100 years with climatological SST and sea ice (with seasonal variation) in order to focus attention on the importance of land surface processes in the climate simulation. The integration shows a well established equilibrium climate state (in the statistic sense). Thus, we take the last 25-year averages as the sufficiently equilibrium climate because they are far away from and are not affected by the initial conditions. Note that the

interannual variation of SST does affect the interannual variabilities of the monsoon system, but it is neglected in our present study.

The paper is organized as follows. In Section 2, we provide a short summary of the IAP two-level AGCM and the coupled new land surface parameterization scheme. In Section 3, the simulated and observed climatology of Asian summer monsoon is presented. In Section 4, the seasonal variation of Asian monsoon is described. The summary and conclusions are presented in Section 5.

II. MODEL AND DATA DESCRIPTION

1. *The Model*

The IAP94 GCM is a grid-point model with a grid spacing of 4° of latitude by 5° of longitude with two interior tropospheric levels (no stratosphere is included). The detailed description of the this AGCM can be found in Zeng et al. (1989) and Dai & Zeng (1997), its main aspects are briefly summarized in Table 1.

2. *The Data*

The simulated data used in this paper are the last 25 years of 100-year integration carried out with IAP94-GCM. The model precipitation climatology is compared with the observation from Jaeger (1976), other variables are compared with a 13-year climatology derived from NCEP / NCAR reanalysis (hereafter referred to as reanalysis) for the period of 1982-1992 (Kalnay et al., 1996).

III. SIMULATION OF THE ASIAN SUMMER MONSOON

In this section, the summer large-scale features of wind, temperature and OLR fields simulated by IAP94-GCM are shown and compared with the observations.

The 850 hPa global summer wind of the model and the reanalysis are displayed in Fig.1. In the observation at 850 hPa the prominent wind systems are the cross-equatorial flow along the east coast of Africa and the easterly trade winds in the tropical Pacific. Under the effect of the Coriolis force, the cross-equatorial flow becomes the southwest monsoon in South Asia and meets with another cross-equatorial flow in the vicinity of South China Sea and with the trade winds in the western tropical Pacific. Over the Indian Ocean, the Somali jet and the upstream flow from the Mescarene High near 90°E, 30°S are well developed. The anticyclonic gyre over the Indian Ocean is very pronounced. In the subtropics, the anticyclone (subtropic high) is well developed and becomes localized over the northeastern Pacific. This is related to the establishment of the northern summer quasi-stationary wave-vortex patterns, in part, by the thermal contrast between the hot interior land mass of Asia and North America and the cooler subtropical Pacific. In general these features are well simulated by the model, except that (a) the model winds are somewhat greater than the observed ones over the west coast of Pacific and over Eurasia near the northwestern Pacific; (b) the location of the belt of westerlies in the Southern Hemisphere is displaced northward about 5-10° relative to the observation (this is clearly a model deficiency resulting in the strong cross-equatorial flow over the Indian Ocean and probably is due to the low horizontal resolution of our model).

The 200 hPa global summer wind of the IAP94-GCM and the reanalysis are shown in Fig.2. In the observation at 200 hPa, the most outstanding features are the huge anticyclonic

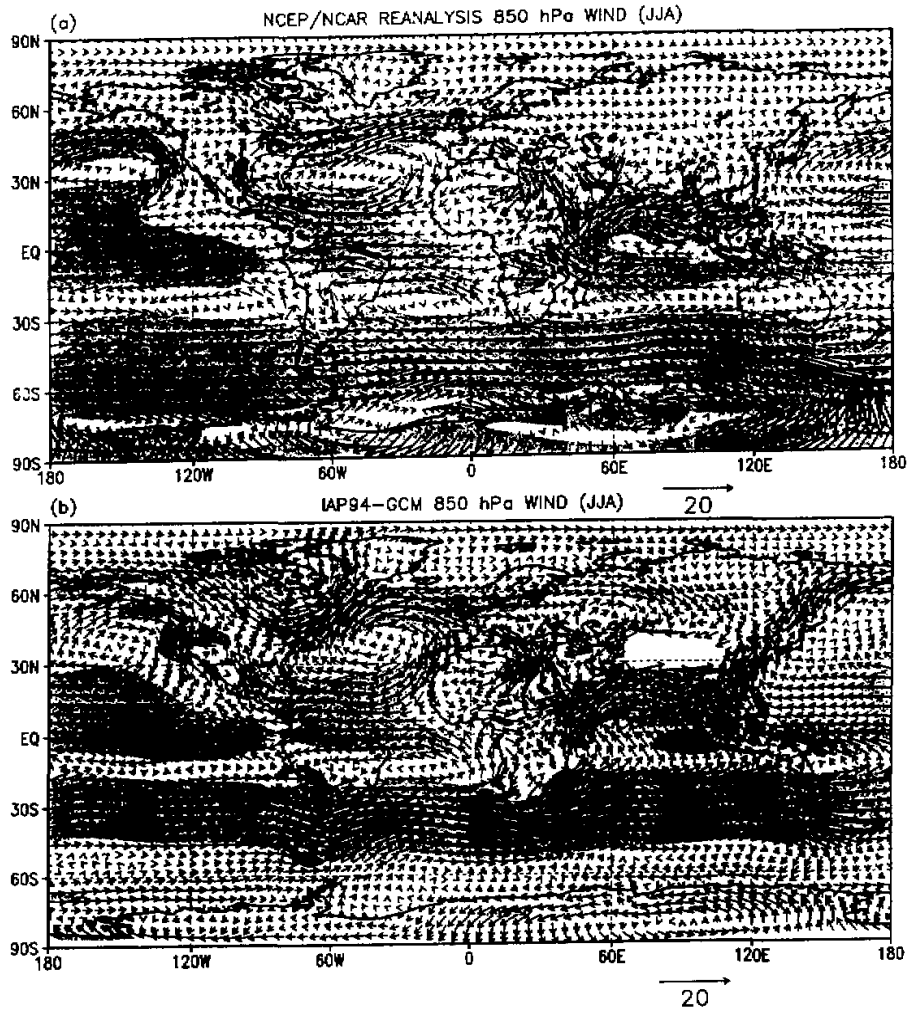

Fig.1. The summer (June–August) global 850 hPa wind climatologies (ms^{-1}). (a) NCEP / NCAR reanalysis. (b) Model simulation. The shaded regions indicate the magnitude of wind greater than 5 m / s.

circulation (Tibetan High) centered over the southern edge of the Tibetan Plateau and extended eastward and westward, and the strong cross-equatorial flow from the Northern Hemisphere to the Southern Hemisphere along the eastern and southern periphery of the Tibetan High. The simulation is in general agreement with the reanalysis. However, (a) the simulated subtropical westerly jet in the Northern Hemisphere appears slightly weaker and extends to a wider range, and (b), the westerlies in high-latitude are much stronger than the observation. The mechanism leading to the stronger wind in the simulation is unknown yet.

Fig.3 shows the observed and simulated summer mean distributions of OLR fluxes. The regions with OLR values less than 240 W / m^2 are shaded. In the observation in the tropics,

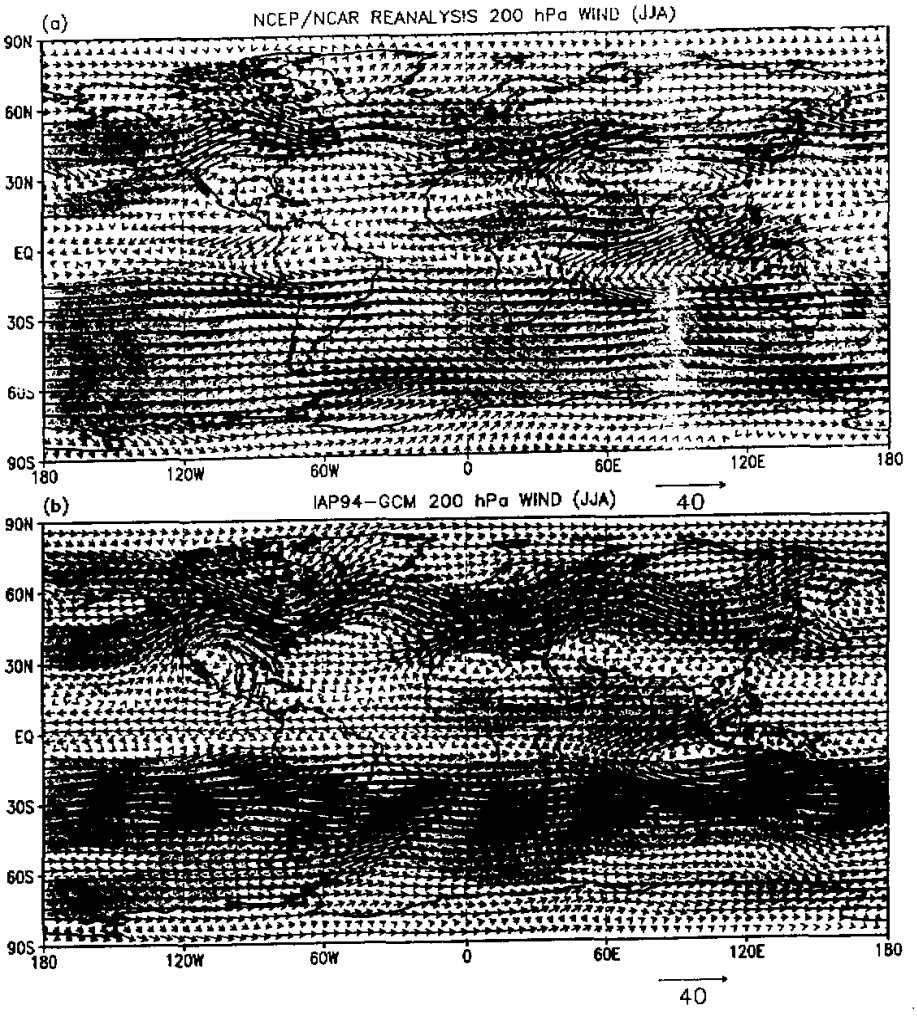

Fig. 2. The same as in Fig.1 but for 200 hPa. The shaded regions indicate the magnitude of wind greater than 10 m / s.

the region where the OLR flux less than 240 W / m^2 indicates the existence of deep cumulus convection. However, in the high latitude and high altitude regions, low OLR values may indicate the cold ground surface temperature. The organized deep convection (implying heavy precipitation) is mainly confined over the Asian southwesterly monsoon region and the western Pacific warm pool, with the eastward extension to the ITCZ in the eastern Pacific and Central America. Deep convection is also found over Tropical Central Africa. Over the cloud-free regions under larger-scale subsidence, such as in the South Indian Ocean (south to 10°S), the northeastern and southeastern Pacific north to 30°S in the Southern Hemisphere, and the northern and southern Atlantic, the OLR values are greater than 260 W / m^2. Very large OLR values

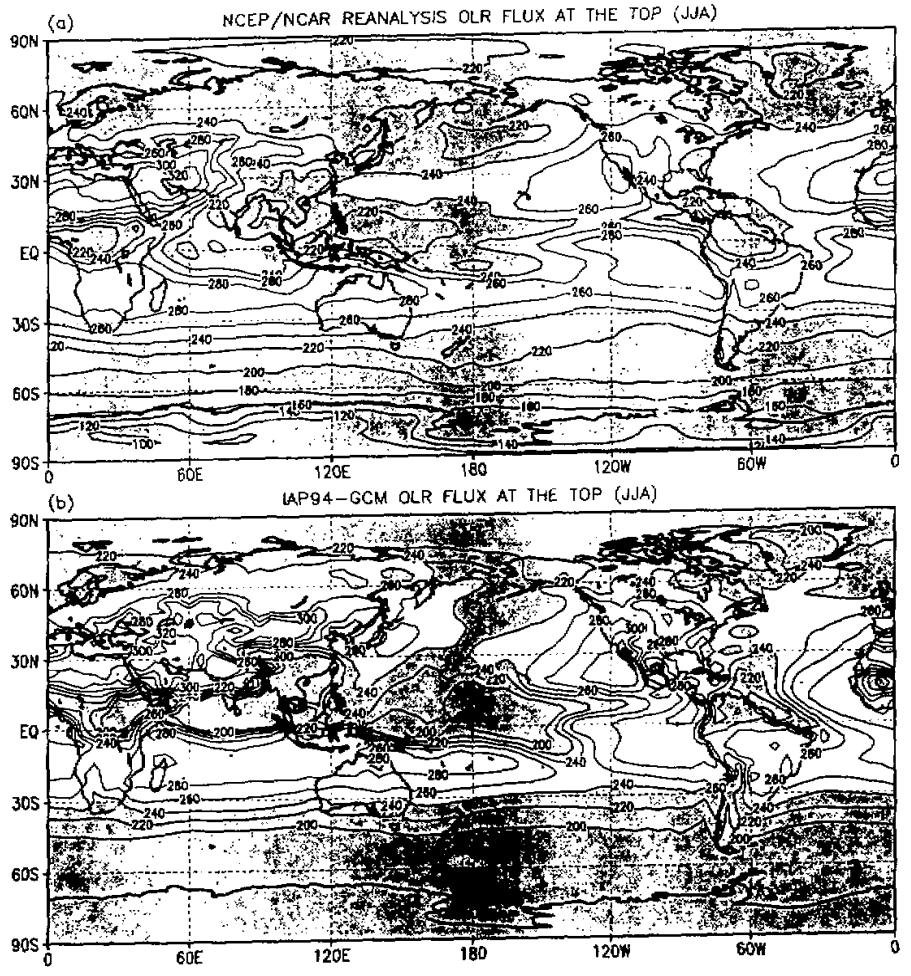

Fig. 3. The summer (June–August) mean OLR flux (W / m^2). (a) NCEP / NCAR reanalysis. (b) Model simulation. The shaded regions indicate the OLR flux less than 240 W / m^2.

(300 W / m^2) are found over very dry land areas including the Sahara Desert, the Saudi Arabian Desert, and the Iran–Afghanistan region, with extension to the western China and Mogolia and coincide with high ground surface temperature there. These features are well reproduced. But in the simulation, (a) the values are somewhat lower than the reanalysis and occupy a slight larger area near the ITCZ; (b) the high OLR values also cover most of Eurasian continent, which result in higher simulated surface temperature and lower cloudiness (Dai, Xue and Zeng, 1997); and (c) the high OLR values occur in the northern Indian subcontinent and Tibetan Plateau. (As a result, a less summer rainfall is simulated in those areas and may be due to the low horizontal resolution of the model, hence the plateau is too wide and too low in the model and is not able to produce heavy precipitation in the south of the high mountain edge).

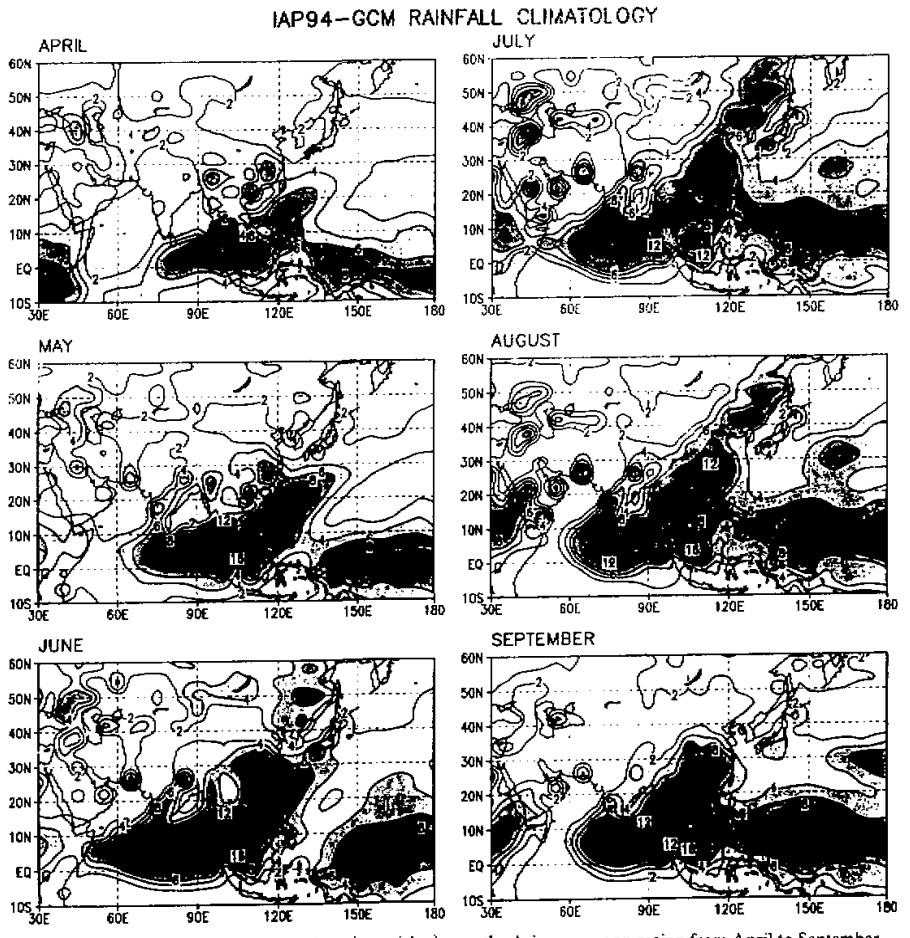

Fig. 4. IAP 94-GCM rainfall climatology (mm / day) over the Asian monsoon region from April to September.

IV. SIMULATION OF SEASONAL VARIATIONS OF ASIAN MONSOON

1. *Rainfall*

The monthly distributions of IAP94-GCM monsoon rainfall for April through September and the observed ones (Jaeger maps) are shown in Fig.4 and Fig.5 respectively. During April, the simulated maximum rainfall is confined to the near-equatorial 5°N near Malaysia, and a large rainfall area extends eastward from it to the southern part of South China Sea and Philippines and westward to 5°N over the eastern Indian Ocean. In the subtropics, the area under the influence of the anticyclone, rainfall is very small or even absent. By comparison, the Jaeger rainfall map (Fig.5) indicates a less active near-equatorial ITCZ but more active premonsoon subtropical rainbelt over the coast of East Asia and extended to the southern tip of Japan due to the cyclone activity in the westerlies. This means that the onset of simulated monsoon rainfall is earlier than the observed although the general feature of the rainfall belt is well simulated.

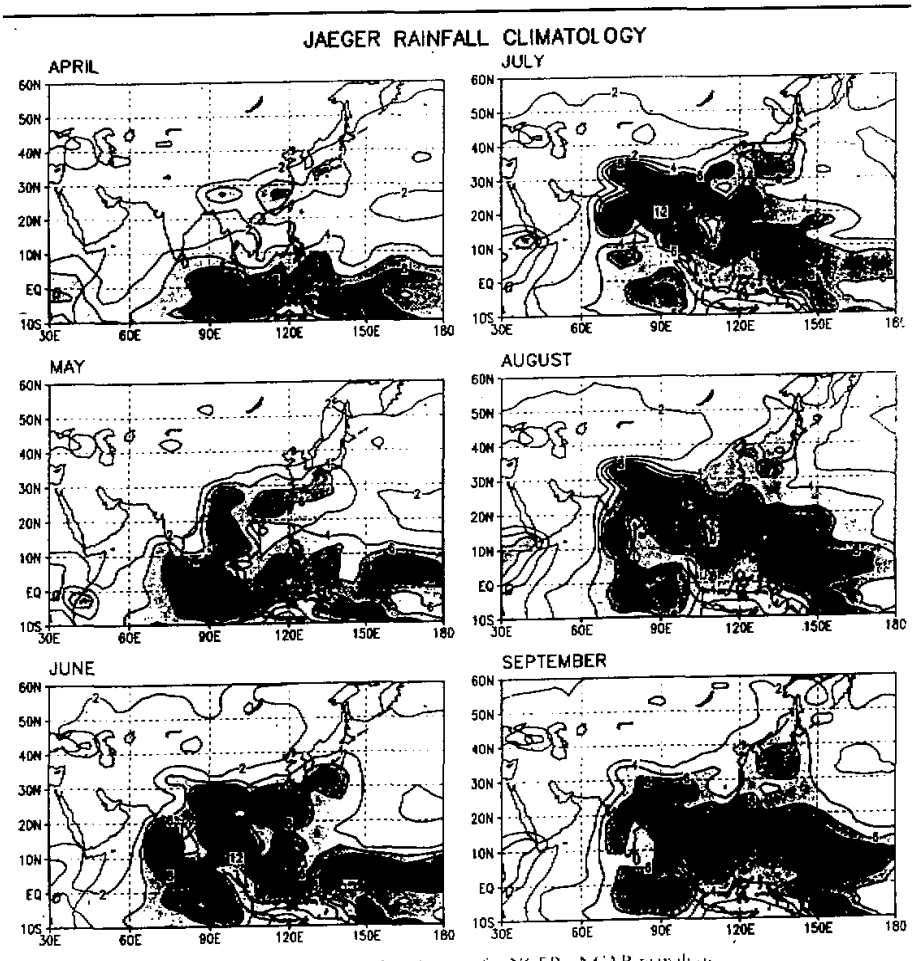

Fig. 5 The same as in Fig. 4 except for NCEP–NCAR reanalysis.

In May, the simulated ITCZ is well developed but its axis still maintained in 5°N. Barely noticeable is the northeastward extension of a secondary rainband from Indo–China across south coast of East Asia, this is the early Mei–yu rainband. Note that this is not the exact Mei–yu rain, but it is called as the Longzhou rain (Dragon Boat rain) lasted from the middle May to the early June. Dragon Boat is a sport game for memorizing a great Chinese patriot and poet Qu Yuan. In the Jaeger rainfall map, this early Mei–yu rainband is slightly stronger than the simulated one. However, the rainfall belt located at the eastern coastal region of the Bay of Bengal is wider and stronger in the observation than in the simulation. Instead the simulated maximum rain is still located in Malaysia, but it is weak down in the observation.

In June, the model rainfall pattern is characterized by a strong rain maximum over the west coast of the Indian subcontinent, the southern part of the Bay of Bengal and another maximum rain belt located in the eastern China along 25°–35°N and extended to Korea and Japan (The Mei–yu rain). These are consistent with the Jaeger rainfall map. Besides, the rain belt associated with the ITCZ in the western Pacific is located along 5°N both in the simulation and observation. The major discrepancy is that the simulated maximum tends to

stay closer to the equator. Another model deficiency is that rainfall over the Tibetan Plateau is not well developed in the simulation. These two deficiencies probably are also due to the low horizontal resolution and the unsatisfactory representation of the Plateau.

In July, the observed rainfall regions are enlarged and combined as a whole area occupying Indian Peninsula, the Tibetan Plateau, Indo-China, the whole eastern China and extended to Korea and Japan, indicating that the Indian South-west monsoon and the East Asian monsoon are combined as a large monsoon system. Besides, the rain belt associated with the ITCZ in the western tropical Pacific is enhanced and moves to along 10°N. The simulation very well captures all these features, except for too far extension of the eastern Asia monsoon rain belt up to even far away from Northeast China and the too small rainfall in the Bengal Bay region. The later is probably due to the low resolution of the model and bad representation of the plateau, but the cause of the first deficiency is difficult to be interpreted.

In August, the precipitation patterns are similar to the July ones, except for the further advance of rain region into the Northeast China in the observation and the slight wider ITCZ rain region in the western Pacific (the rain region also moves slightly to the north than the July case). It is worth noting that these features are well simulated by the model except that the rain region in Northeast China exists already in July.

In September, both in the observation and simulation the East Asia monsoon rain belt and the ITCZ rain belt move down to the south, and the India monsoon rain region is weakened. However, in the simulation over the Tibetan Plateau and northern India peninsula it is too dry.

Note that there is an abrupt jump of Mei-yu along the Yangtze River to the North China along 40° in the middle July according to many Chinese results of investigation (see, for example, Zeng et al., 1994). However this feature cannot be presented by the monthly mean precipitation maps, unless the averaging period should be shorter somewhat like 10 to 15 days.

2. *Low- and Upper-level Circulations*

The onset of the Indian summer monsoon is marked by the establishment of a southwesterly flow at lower levels and an easterly flow at upper levels over the North Indian Ocean and Southeast Asia. But the onset of eastern Asia monsoon occurs earlier, it is characterized by a cross-equator flow and the south westerly flow at the lower levels in the vicinity of South China Sea. In Fig. 6 we present the reanalysis and the simulated longitude-time section at 15°N showing the mean annual cycle of the intensity of zonal and meridional wind component at 850 hPa, westerlies and southerlies are shaded respectively. From May to September in the observation the westerlies at this level are found only over longitudes covering from the North Africa to South China Sea (between 0° and 120°E). The southwesterlies of moderate intensity first appear in the Bay of Bengal and Southeast Asia in the middle May, and then occupy the Arabian Sea (between 50°E and 70°E) and extend to the western Pacific (up to 180°E) in early June. In summer the strong westerlies occur in the Arabian Sea and continuously extend to the coast of the western Pacific, it is first set up in the vincitity of South China Sea in April to May, although its maximum is located along 60°E in July. The westerlies disappear by the end of September. Although the simulated southwesterlies tend to increase from winter to summer, evidently there exists a stationary westerly throughout the year in the simulation. The model poorly reproduces the onset and withdrawal of the westerly (Note that not only our model but also most of the models in the world possess the same inefficiency and too strong cross-equator flow over the Indian Ocean). The simulated

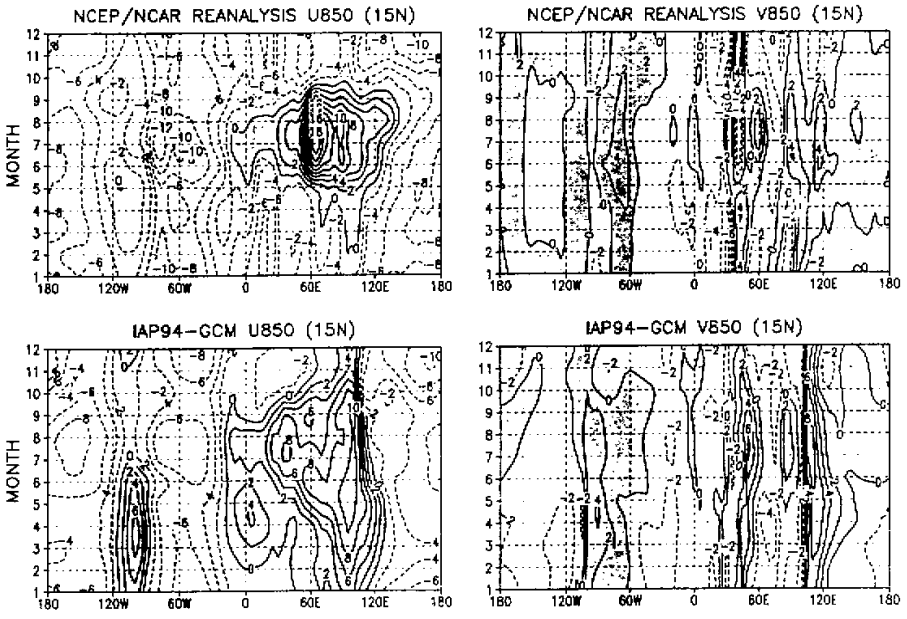

Fig. 6. Latitude-time sections at 15°E showing the NCEP / NCAR reanalysis (upper) and simulation (lower) of the monthly mean zonal wind component (m / s) at 850 hPa, westerly wind is shaded (left); and of menridional wind component, southerly wind is shaded (right).

southerly is in good agreement with the reanalysis except for much stronger southerly over South China Sea.

The longitude-time sections of the observed and simulated 200 hPa mean zonal and meridional wind velocity at 15°N are shown in Fig.7. In the observation intensive easterlies (< -10 m / s) occur between 60° and 150°E during the summer months. The zonal wind in this sector rapidly changes from westerlies to easterlies in the middle of May and attains intensity maximum in July and August and then gradually changes from easterlies back to westerlies in fall. The transition from westerlies to easterlies occurs first in Southeast Asia (near 100°E). Weak easterlies associated with the Mexican high are also found over the tropical eastern Pacific (between 140°W and 90°W). The model well reproduces above features except for the strength of zonal wind is weaker than that of the reanalysis. The simulated meridional wind is in good agreement with the reanalysis. In general, the simulated wind at 200 hPa is much better than that at 850 hPa.

Note that the abrupt seasonal change in the location of westerlies jet at 200 hPa exists both in the observation (Yeh et al., 1959) and simulation (Zeng et al., 1988) in the latitude-time cross-section, and the abruptness is very clear if the averaged time is 10 to 15 days.

3. *Upper-tropospheric Temperature*

Fig.8 shows the observed and simulated longitude-time sections of the difference of the mean upper-tropospheric (200-500 hPa) temperature between 5°N and 30°N, the positive values are shaded. In the observation the reversal of the meridional temperature gradient

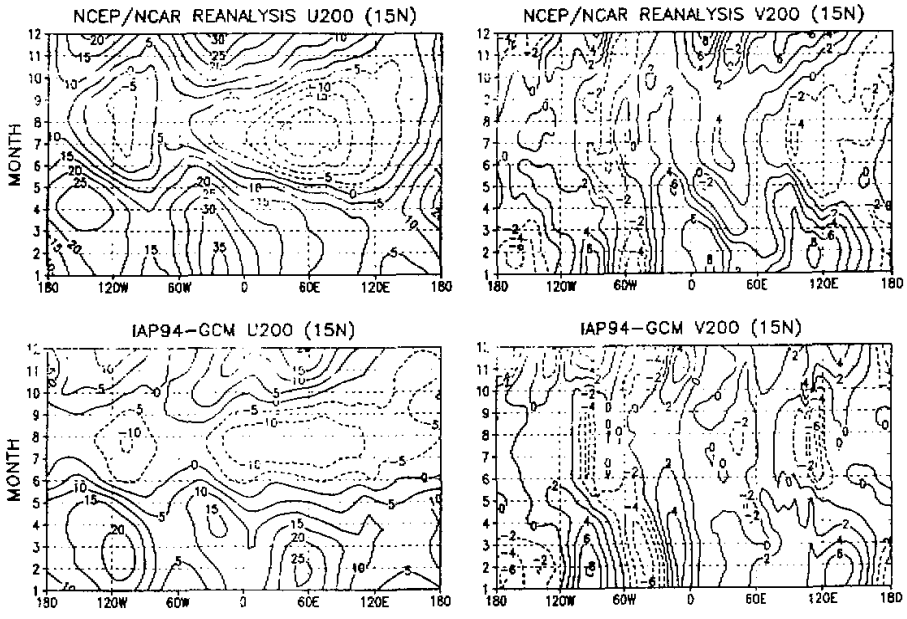

Fig. 7. The same as in Fig. 6, but for 200 hPa.

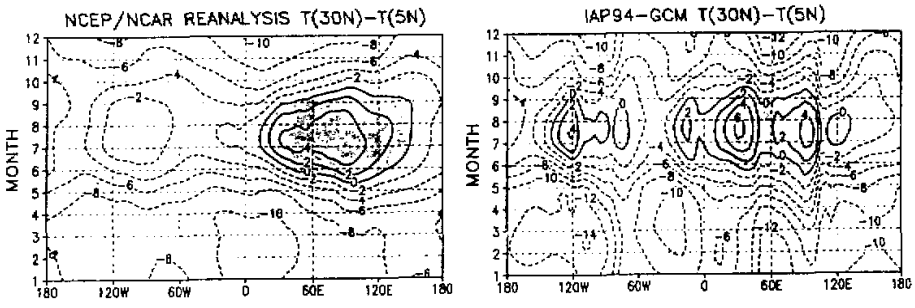

Fig. 8. Longitude-time sections showing the NCEP / NCAR reanalysis (upper) and simulation (lower) of the monthly mean upper-tropospheric (200-500 hPa) temperature (°C) at 30°N minus that at 5°N. The areas of positive values are shaded.

occurs first on the southern side of the Tibetan Plateau (near 90°-100°E) and then expands over a large area extending from Africa to the western Pacific. The temperature difference attains the maximum value in July and becomes negative at the middle of September. The transition of the temperature gradient between positive and negative values corresponds to the typical abrupt change of circulation over East Asia during June and October. The model has successfully reproduced the general feature of these seasonal changes of the difference of the mean upper-tropospheric temperature. However, the simulated values appear somewhat larger than the reanalysis, and the location of positive gradient is somewhat shifted westwards compared with the observation.

4. *Surface Heat Fluxes in Subtropical Zone*

In this sub-section, the seasonal variations of surface heating flux together with the net radiation, sensible heat and latent heat over the subtropical zone (27.5–37.5°N), where the Tibetan Plateau, Iran Plateau, East China and West Pacific are located, are discussed.

The observed and simulated evolutions of the net surface heating flux are shown in Fig.9. In both the reanalysis and the simulation, there exists a strong seasonal variation of surface heating over the western Pacific and a weak variation over the Mediterranean, they show that the large cooling and warming alternatively appear in winter and summer. The maximum centers are in East China Sea and the area of Kuroshio current. However, the simulation is poorly consistent with the reanalysis. Over the land, although the surface heating flux is always small throughout the year in both the observation and simulation. Especially the simulation shows a weak warming except in spring in the Tibetan and Iran Plateaus. It is interesting to note that the seasonal variation over the subtropical continent is more unclear compared with that over the ocean, this means that the land thermal conditions are much more responsive to the net radiation from the atmosphere than the oceans. In reality, land provides much less heat capacity and negligible horizontal transport than the ocean, this results in more variable and changeable surface temperature, moisture and sensible heat exchange.

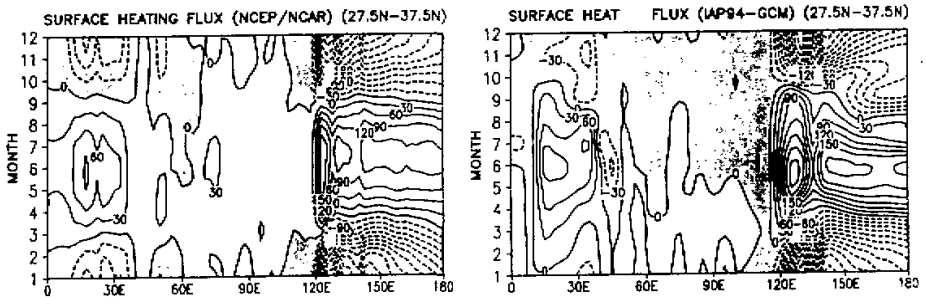

Fig. 9. The NCEP / NCAR reanalysis (upper) and simulation (lower) fot the net surface heating flux (W / m^2) averaged over the band 27.5 to 37.5°N (contour interval is 30 W / m^2), the areas of negative values are shaded.

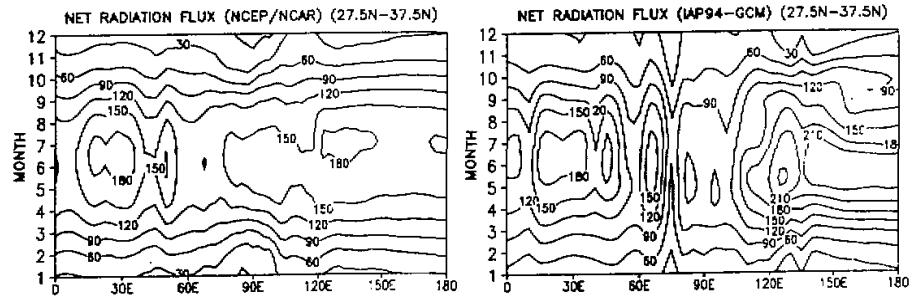

Fig. 10. The same as in Fig.9 except for surface absorbed net radiation flux.

The observed and simulated evolutions of the surface absorbed radiation flux are shown in Fig.10. Both the reanalysis and the simulation show gradually increase of the net absorbed radiation from winter to summer except for a large lag in Pamirs in the simulation compared with the reanalysis. In summer, the large net absorbed radiation centers are found in East China Sea and the Mediterranean. The reversal gradient from land to ocean occurs in the east and west side of Eurasian continent in this season. These features are well simulated by the model, but the seasonal variation in the model is stronger over the western Pacific than that in the reanalysis. In contrast, the simulation shows a relatively weak change and low absorption in Afghanistan due to high surface temperature and large outgoing longwave radiation at the surface, and in the Tibetan Plateau due to a prolongation of snow cover and high surface reflection (figures not shown here). As a result, in the simulation there appears a larger than the reanalysis reversal gradient from land to sea in summer.

The observed and simulated evolutions of the surface sensible heat flux are shown in Fig.11. Both the reanalysis and the simulation show an apparent seasonal variation of surface sensible heat flux. In the reanalysis over the western Pacific, an upward flux occurs in winter and a downward flux in summer. In contrast, over the Tibetan Plateau a weaker downward flux occurs in winter, and a larger upward flux in summer. The large surface heat fluxes occur in the eastern and western part of the Plateau. The simulation shows two centers more clear than the reanalysis. The eastern center is intensified from the beginning of April before the onset of monsoon (This means why the simulated onset of the summer monsoon is somewhat earlier than the observed one). Along the eastern coast of the Asian continent, the reversal gradient of sensible heat flux occurs at the same time. Since then such a thermal contrast between land and sea has changed completely. The surface sensible heating by the Plateau certainly plays some roles in the seasonal transition of at least the surrounding regions and in the onset of the Asian monsoon. The simulated upward flux over the west of 70°E is much smaller than that of the reanalysis. Another deficiency of the simulation is that there exists an upward sensible heat flux throughout the year over the Tibetan Plateau, while in the reanalysis there exists a weaker downward flux in winter.

The observed and simulated evolutions of the surface latent heat flux are shown in Fig.12. In the area of west of 75°E, the reanalysis gives a less surface latent heat flux (basically below 60 W/m^2) throughout the year. But in the simulation, two anomalous high value centers appear in summer, one is located in Iraq and another in Afghanistan. This might be resulted from the bad simulation of precipitation in those regions due to the bad representation of the plateau in the model. Before the monsoon onset, there exists a general tendency of increase of latent heat flux from land to sea over East Asia. After the monsoon onset, the surface latent heat flux over western Pacific becomes weaker. The large surface latent heat fluxes are located in the plateau and the coast of East China. The contrast between land surface and sea surface reverses completely. The simulation is in good agreement with the reanalysis in this transition.

V. SUMMARY AND CONCLUSIONS

We have examined the ability of the IAP94–GCM to simulate the seasonal variations, especially the Asian monsoon. Generally speaking, the model well simulates the spatial and temporal variabilities of the basic features of the seasonal variation of the general circulation and surface variables and the Asian monsoon. These include the evolution of the global-scale atmospheric circulation, rainfall, and various components of the surface heat fluxes.

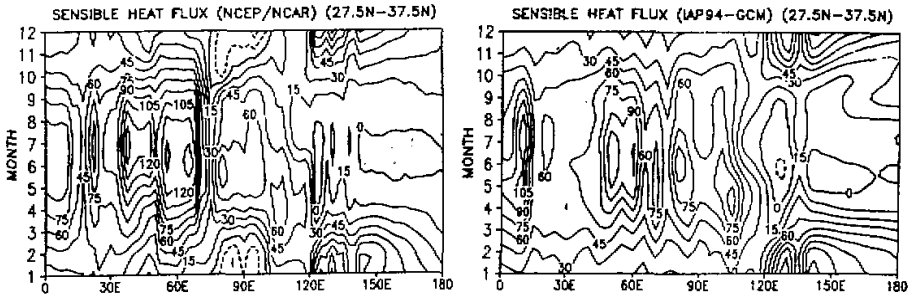

Fig. 11. The same as in Fig. 9 except for surface sensible heat flux (contour interval is 15 W / m^2), the areas of negative values are shaded.

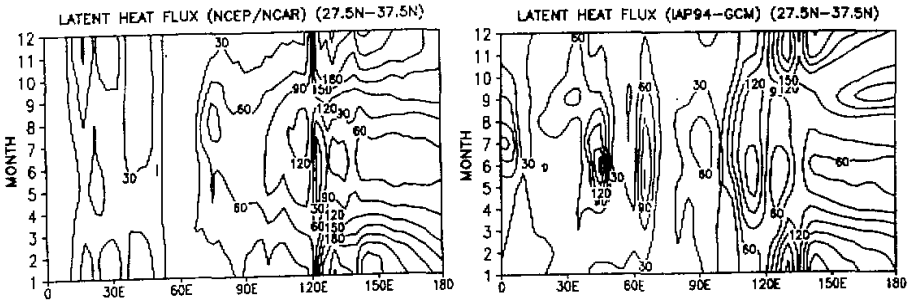

Fig. 12. The same as in Fig. 9 except for surface latent heat flux (contour interval is 30 W / m^2), the areas of values greater than 120 are shaded.

All our results show that the land surface processes are very important for correctly simulating the seasonal variation, especially Asian monsoon, this also leads us to have a better understanding of the Asian monsoon.

IAP94-GCM has successfully reproduced the seasonal variation of surface heat fluxes in subtropics. It is indicated that the seasonal variation of general atmospheric circulation is primarily caused by the seasonal change of the incoming solar radiation, in addition, the surface sensible and latent heat fluxes show reversal and strong seasonal variations between the land and sea over the subtropic region, so that the increases of land heat fluxes from winter to summer are also important in the formation and evaluation of the Asia monsoon.

Interannual variability of the entire monsoon system, of course, is affected also by the interannual variation of SST, but it is excluded in our present study by using a prescribed climatological mean SST (with seasonal variation) in our simulation. It is the subject of a subsequent study using a global coupled land-ocean-atmosphere GCM.

The authors are very grateful to Wang Xuan for typing this paper.

REFERENCES

Arakawa A., Katayama A., and Y. Mintz (1969), Numerical simulation of the general circulation of the atmosphere, *Proceedings of the WMO / IUGG Symposium on Numerical Weather Prediction*, Tokyo, Japan Meteor. Agency.

pp. IV-7 to IV-8-12.

Barnett T.P., Dumenil L., Schlese U., Roeckner E., and M. Latif (1989), The effect of Eurasian snow cover on regional and global climate variations, *J. Atmos. Sci.*, **46**: 661-685.

Cess R.D. (1985), Nuclear war: Illustrative effects of atmospheric smoke and dust upon solar radiation, *Climate Change*, **7**: 237-251.

Cess R.D. and G.L. Potter (1987), Exploratory studies of cloud radiation forcing with a general circulation model, *Tellus*, **39A**: 460-473.

Cess R.D., Potter G.L., Ghan S.J., and W.L. Gates (1985), The climate effects of large injections of atmospheric smoke and dust: A study of climate feedback mechanisms with one- and three-dimensional climate models, *J. Geophys. Res.*, **90**: 12937-12950.

Dai Y.J. and Q.C. Zeng (1997), A land surface model (IAP94) for climate studies, Part I: Formulation and validation in off-line experiments, *Advances in Atmospheric Sciences*, **14**: 433-460.

Dai Y.J., F. Xue and Q.C. Zeng (1998), A land surface model (IAP94) for climate studies, Part II: Implementation and preliminary results of coupled model with IAP AGCM, *Advances in Atmospheric Sciences*, **15**: 47-62.

Dorman J.L and P.J. Sellers (1989), A global climatology of albedo, roughness length and stomatal resistance for atmospheric general circulation models as represented by the simple biosphere model (SiB), *J. Appl. Meteor.*, **28**: 833-855.

Douville H. and J.F. Royer (1996), A new snow parameterization for Sensitivity of the Asian summer monsoon to an anomalous Eurasian snow cover within the Meteo-France GCM, *Clim. Dyn.*, **12**: 449-466.

Gates W.L. and A.B. Nelson (1975), A new tabulation of the Scripps topography on a 1° global grid, Part I: Terrain heights, R-1276-1-ARPA, The Rand Corporation, Santa Monica, CA, 132 pp.

Jaeger L (1976), Monatskarten des Niederschlag fur die ganze Erde, *Berichto des Deutschen Wetterdienstes*, Nr. 139, pp 38.

Kalnay E., coauthors (1996), The NCEP/NCAR 40-year reanalysis project, *Bull. Amer. Meteor. Soc.*, **77**: 437-471.

Katayama A. (1972), A simplified scheme for computing radiative transfer in the troposphere, Tech Rep No.6, Department of Meteorology, University of California, Los Angeles, CA, 77 pp.

Lau K.-M. and S. Yang (1996), Seasonal variation, abrupt transition, and intraseasonal variability associated with the Asian summer monsoon in the GLA GCM, *J. Clim.*, **9**: 965-985.

Li C. and M. Yanai (1996), The onset and interannual variability of the Asian summer monsoon in relation to land-sea thermal contrast, *J. Clim.*, **9**: 385-375.

Lin Z.H., Q.C. Zeng and B. Ouyang (1996), Sensitivity of IAP 2L AGCM to surface albedo variation, *Theoretical and Applied Climatology* (Special Issue), 157-162.

Meehl G.A. (1994), Influence of the land surface in the Asian monsoon: External conditions versus internal feedbacks, *J. Clim.*, **7**: 1033-1049.

Smagorinsky J (1963), General circulation experiments with the primitive equations, I: The basic experiment, *Mon. Wea. Rev.*, **93**: 99-164.

Vernekar A.D., Zhou J., and J. Shukla (1995), The effect of Eurasian snow cover on Indian monsoon, *J. Clim.*, **8**: 248-266.

Wilson M.F. and A. Henderson-Sellers (1985), A global archive of land cover and soil data for use in general circulation climate models, *J. Climatol.*, **5**: 119-143.

Yang S., Lau K.-M., and M. Sankar-Rao (1996), Precursory signals associated with the interannual variability of the Asian summer monsoon, *J. Clim.*, **9**: 949-964.

Yasunari T., Kitoh A., and T. Tokioka (1991), Local and remote responses to excessive snow mass over Eurasian appearing in the northern spring and summer climate - a study with the MRI GCM, *J. Meteor. Soc.* Japan, **69**: 473-487.

Yeh T.C., S.Y. Tao and M.T. Li (1959), The abrupt change of circulation over the Northern Hemisphere during June and October, in the Atmosphere and the Sea in Motion, 249-267.

Zeng Q.C., X.H. Liang and M.H. Zhang (1988), Numerical simulation of the monsoon and the abrupt seasonal change in general atmospheric circulation, *Chinese Journ. Atmos. Sci.*, Special Issue, 22-42. (in Chinese)

Zeng Q.C., Zhang X.H., Liang X.Z., Yuan C.G., and S.F. Chen (1989), Documentation of IAP two-level Atmospheric General Circulation Model, TR044, DOE / ER / 60314-HI, 383 pp.

Zeng Q.C., Zhang B.L., Liang Y.L. and Zhao S.X. (1994). East Asian summer monsoon-a case study, *Proc. Indian Natn. Sci. Acad.*, 60, A, No.1, 81-96.

Zeng Q.C., Yuan C.G., Li X., Zhang R.H., Yang F.L., Zhang B.L., Lu P.S., Bi X.Q. and H.J. Wang. (1997), Seasonal and extraseasonal predictions of summer monsoon precipitation by GCMs, *Advances in Atmospheric Sciences*, **14**: 163-176.

Zwiers F.W. (1993), Simulation of the Asian summer monsoon with the CCC GCM-1, *J. Clim.*, **6**: 470-486.